Supporting Information

Roston et al. 10.1073/pnas.1000931107

SI Text

SI Materials and Methods. *Kinetic experiments.*

Materials.
All chemicals were from Sigma unless otherwise specified. 2° kinetic isotope effects (KIEs) on the yeast alcohol dehydrogenase (yADH)-catalyzed reduction of benzaldehyde by NADH were measured competitively in conditions meant to mimic those used in other studies of this system (1). Competitive measurements use two different isotopically labeled substrates in the same reaction vessel and measure the enrichment of one of the isotopologues in the products at various time points. In the case of the H/T KIE (cf. k_H/k_T) for benzaldehyde reduction, [7-^{3}H]-benzaldehyde and [ring-^{14}C]-benzaldehyde (as a trace for ^{1}H) served as the labeled substrates. [ring-^{14}C]-benzaldehyde was commercially available (American Radiolabeled Chemicals) and [^{3}H]-benzaldehyde was produced by reduction of benzoyl chloride by [^{3}H]-$NaBH_4$ (American Radiolabeled Chemicals) in the presence of Cd^{2+} according to an adaptation of a published procedure (2). D/T KIE experiments (cf. k_D/k_T) used [ring-^{14}C-7-^{2}H]-benzaldehyde (as a trace for D), which was produced by CN^- catalyzed exchange of the aldehydic proton with D_2O by an adaptation of a published procedure (3). *R*-[4-^{2}H]-nicotinamide adenine dinucleotide (NADD) was used for experiments with D transfer and it was synthesized by reduction of NAD^+ with EtOH-d_6 by yADH (4).

Enzyme preparation.
Whereas most previous studies (1, 5–8) used commercially available yADH, a recent report found that commercially available materials are mixtures of isozymes, only one of which is active toward aromatic substrates (9). The aromatic-active isozyme, yADH 2, was expressed and purified as described previously (10) in a strain of yeast deficient in genes for the other isozymes (a generous gift from Bryce V. Plapp from the University of Iowa, Department of Biochemistry).

Kinetic measurements.
Prior to each reaction, synthesized [^{3}H]-benzaldehyde was copurified with the [^{14}C]-benzaldehyde (either H or D at the aldehydic position) by HPLC over a C-18 column (4.6 × 250 mm) at 1 mL/min in 25:75 MeCN:H_2O. The final 1-mL reaction mixtures, meant to mimic the conditions of ref. 1, contained 2 mM benzaldehyde (300,000 dpm ^{14}C and 1,500,000 dpm ^{3}H), 80 mM glycine (pH 8.5), 20 mM NADH (or NADD), and sufficient enzyme to reach complete conversion to products within a few hours. Reactions were initiated by addition of the enzyme and maintained at 25° until quenching with 10 mM $HgCl_2$ at a range of time points. Samples were frozen at −80 °C until ready for HPLC analysis.

Reactants and products were separated by C-18 HPLC using the method above and collected in 1-min fractions. In these conditions, benzyl alcohol elutes at 8–9 min and benzaldehyde at 15–16 min. The ^{14}C and ^{3}H contents of the fractions were measured by liquid scintillation counting with a Packard TriCarb 2900TR liquid scintillation analyzer. KIEs were calculated according to

$$\mathrm{KIE} = \frac{\log(1-f)}{\log(1-fR_p/R_0)}, \qquad \textbf{[S1]}$$

where f is the fractional conversion to products, R_p is the isotopic ratio in the products, and R_0 is the initial isotopic ratio in the reactants (11).

Computational modeling. All geometry optimizations, calculations of vibrational frequencies, and potential energy surface (PES) scans were done with density functional theory using *GAUSSIAN 03* at the B3LYP level (12). Although no solvent model was used, the calculations are not "gas-phase" calculations, as geometric restrictions were imposed to fit the kinetic data and represent the enzymatic/solvent environment. Following the footsteps of other empirical models of this type (13–17), the geometrical parameterization bypasses the need to explicitly include solvent, active site, or other environmental effects in the calculations. The chosen level of theory gave good initial results for the equilibrium isotope effects (EIEs), suggesting that it was suitable to model vibrational changes over the course of the reaction. The model incorporated a total of 43 atoms, which were the same atoms used in another model of the ADH-catalyzed reaction (18), and included the entire benzyl substrate, the catalytic zinc and its ligands, and the nicotinamide moiety of the cofactor. The ground state structures for both forms of both substrates (benzyl alkoxide, benzaldehyde, NAD^+, and NADH) were treated separately and completely optimized to their equilibrium geometries (Fig. S1), aside from some dihedral angles around the catalytic zinc and the Zn-O bond distance, which were constrained to match the newly available crystal structure of yADH [Protein Data Bank (PDB) ID code 2HCY] and a structure of hlADH with an aldehyde analogue (PDB ID code 1LDY).

To assess the tunneling ready state (TRS) for this system, we assumed that the 1° hydride cannot be modeled classically and is delocalized between the reactant and product wells in accordance with Marcus-like models of hydrogen tunneling (Fig. 2) (19–22). We adapted the method used by Redington to calculate the TRS for the proton transfer in tropolone (23). The 1° hydrogen was frozen directly midway between the donor and acceptor carbons with an angle of 180°. This angle was chosen for computational simplicity, but quantum mechanical/molecular mechanical simulation models demonstrate that the angle indeed does not substantially deviate from linearity (18, 24). The positions of the other 42 atoms in the system were then optimized at a range of donor–acceptor distances (DADs) and Zn-O bond lengths. The optimized geometries for the heavy atom skeleton were then frozen and the hybridizations of the donor and acceptor carbons were parameterized by altering the out-of-plane bend (θ) of the 2° hydrogens (Fig. 1). This parameterization was necessary to give a degenerate double-well potential ($\Delta E_{D\text{-}A} = 0$) in accordance with Marcus-like models of hydrogen tunneling. Each combination of DAD and Zn-O bond length has an ensemble of structures with $\Delta E_{D\text{-}A} = 0$, so the minimum energy point along the $\Delta E_{D\text{-}A} = 0$ surface was taken as the weighted average of the full ensemble of TRS structures. KIEs were calculated at that point for each combination of DAD and Zn-O bond length and compared with experiment to find the best fit.

Calculations of 2° KIEs. To calculate 2° KIEs, we approximated the position of the delocalized hydrogen as a simple linear combination of donor and acceptor positions (Fig. 4):

$$\Psi_{\mathrm{TRS}} \approx \frac{1}{\sqrt{2}}\Psi_d + \frac{1}{\sqrt{2}}\Psi_a, \qquad \textbf{[S2]}$$

where Ψ_{TRS} represents the overall wave function of the TRS, and Ψ_d and Ψ_a represent the wave functions when the hydride is localized in the donor well and acceptor well, respectively. Thus, KIEs were calculated for both the donor (k_{Ha}/k_{Td}) and acceptor (k_{Ha}/k_{Ta}) states according to the Bigeleisen equation (25):

$$\frac{k_{Hd}}{k_{Td}} = \kappa_d \cdot \mathrm{MMI}_d \cdot \mathrm{EXC}_d \cdot \frac{e^{-\beta h\left(\nu_{Hd}^{\ddagger} - \nu_H\right)}}{e^{-\beta h\left(\nu_{Td}^{\ddagger} - \nu_T\right)}}, \qquad [S3]$$

$$\frac{k_{Ha}}{k_{Ta}} = \kappa_a \cdot \mathrm{MMI}_a \cdot \mathrm{EXC}_a \cdot \frac{e^{-\beta h\left(\nu_{Ha}^{\ddagger} - \nu_H\right)}}{e^{-\beta h\left(\nu_{Ta}^{\ddagger} - \nu_T\right)}}. \qquad [S4]$$

Here β is $1/k_BT$, h is Planck's constant, and ν represents the vibrational frequencies of the isotopically labeled molecules at the ground state (ν_H and ν_T) and the donor ($\nu_{Hd}^{\ddagger}$ and $\nu_{Td}^{\ddagger}$) and acceptor ($\nu_{Ha}^{\ddagger}$ and $\nu_{Ta}^{\ddagger}$) states that compose the TRS. The leading terms of these equations (κ, MMI, and EXC) represent isotopic differences in transmission coefficient, mass moment of inertia, and vibrationally excited populations, respectively. These terms do not make significant contributions to 2° KIE, so the overall KIE reduces to

$$\left(\frac{k_{Hd}}{k_{Td}} \cdot \frac{k_{Ha}}{k_{Ta}}\right)^{1/2} \approx \frac{e^{-\beta h\left(\frac{\nu_{Hd}^{\ddagger} + \nu_{Ha}^{\ddagger}}{2} - \nu_H\right)}}{e^{-\beta h\left(\frac{\nu_{Td}^{\ddagger} + \nu_{Ta}^{\ddagger}}{2} - \nu_T\right)}} \approx \frac{k_H}{k_T}. \qquad [S5]$$

The program *ISOEFF07* (26) was used to calculate KIEs based on vibrational frequencies from *Gaussian* (uniformly scaled by 0.95 following the correction suggested by Rucker and Klinman (17)).

Calculations of 1° KIEs. 1° KIEs were estimated assuming that the reaction is vibrationally adiabatic and that the principal sources of the KIE are the change in the C-H(D) stretch vibrational energy (E_v) as the system evolves from the ground state to the TRS and the difference in electronic energy (E_e) between the TRS for H and for D transfer. The 1D PES for the C-H stretch was calculated at the ground state and the TRS for both forward and reverse reactions using a larger basis set (B3LYP/6-31 + G*) to obtain more realistic results near the barrier of the double-well potential at the TRS. Single point energies for 20–25 different positions of the hydrogen were fit (least-squares) to a quartic function at the TRS. For the ground states, initial fits to a Morse-type potential gave noticeable deviations from the calculated points, but an 8th-order polynomial approximation gave a very good fit for the region near the minimum of the PES.

The vibrational zero point energy for each PES was determined numerically by finding upper and lower limits on the energy for which solutions to the Schrödinger equation were convergent. By iteratively narrowing those limits, the eigenvalues of the Hamiltonian could be determined to any precision desired. Using these vibrational energies and their associated electronic energies, KIEs were estimated as

$$\frac{k_H}{k_D} = \frac{\mathrm{Exp}\left[-\beta\left({}^{H}\Delta E_e^{\ddagger} + {}^{H}\Delta E_v^{\ddagger}\right)\right]}{\mathrm{Exp}\left[-\beta\left({}^{D}\Delta E_e^{\ddagger} + {}^{D}\Delta E_v^{\ddagger}\right)\right]}, \qquad [S6]$$

where ${}^{i}\Delta E_e^{\ddagger}$ is the electronic activation energy for isotope i and ${}^{i}\Delta E_v^{\ddagger}$ is the vibrational activation energy for isotope i.

The time (t) required for all of the probability density of the hydride to pass through the barrier at the TRS was calculated according to (27)

$$t = \frac{\hbar}{2\Delta E_{\mathrm{split}}}, \qquad [S7]$$

where $\Delta E_{\mathrm{split}}$ is the tunneling splitting (the energy difference between the ground- and first-excited vibrational states of the tunneling particle). $\Delta E_{\mathrm{split}}$ was calculated by the method described above for determining eigenvalues of the Hamiltonian at the TRS.

Experimental results. Competitive H/T and D/T 2° KIE measurements for the reduction of benzaldehyde by NADH and NADD, respectively, are displayed in Fig. S2. The fact that the measured KIEs are invariant over a large range of fractional conversions indicates that the results are reliable. Importantly, the value measured for the H/T KIE ($1.05 \pm .01$) is within the error reported in a previous measurement of this KIE (7) but is more precise and shows definitively that the KIE is normal (>1), despite the inverse (<1) EIE measured for this reaction. The D/T KIE with D transfer ($1.01 \pm .02$) is within error of unity, though, and the mixed-labeling Swain–Schaad exponent (mSSE) measured for this reaction (4.9 ± 2.0) is within error of the semiclassical value of 3.3. Deviations from the semiclassical mSSE in the forward reaction have served as strong evidence for tunneling in yADH (1), but the large errors associated with the small KIEs in the reverse direction prevent such a conclusion from these data.

Nonetheless, the mere fact that the H/T KIE is normal, despite the inverse EIE, provides strong evidence that tunneling and coupled motion play an important role in the reaction. 2° KIEs outside the range of the 2° EIE to unity are rare, but not unprecedented, especially in enzymatic reactions, and are generally interpreted as evidence for tunneling and coupled motion, without giving significantly deeper analysis (28–31). Other anomalies in 2° KIE measurements in ADH, especially inflated mSSEs, have received a great deal of theoretical treatment (15, 17, 24, 32, 33), but these models have typically failed to address the abnormal KIEs on the nicotinamide cofactor or predicted the previously unavailable KIE reported here. The implications of such KIEs for TRS structure are described in the main text.

Additional discussion regarding ligation to the catalytic zinc. Some of the most striking features apparent from the optimized ground states (Fig. S1) are the changes around the catalytic Zn between reactants and products. The Zn-O bond lengths were constrained during the optimizations to reflect the crystal structure of yADH with trifluoroethanol (PDB ID code 2HCY) and a structure of hlADH with cyclohexyl formamide (PDB ID code 1LDY). The latter structure, which is meant to serve as an analog for the aldehyde, has a Zn-O bond length of 2.3 Å and reflects the trigonal pyramidal geometry around the Zn observed in our optimized aldehyde ground state. The situation in the yADH/trifluoroethanol structure is somewhat more complicated. Although the enzyme is a homotetramer, two of the subunits did not crystallize with a cofactor and exhibit alternative ligation to the catalytic Zn. The two subunits that bound both substrates have a Zn-O bond length of 1.8 Å, which is the value used to constrain the alkoxide ground state in our calculations.

Notably, the changes in ligation around the Zn at the TRS were vital to replicating the KIEs in our model. We explored the whole range of values for the Zn-O bond length between 1.8–2.3 Å and found the best fit to experimental KIEs near the upper limit, at 2.25 Å. In contrast to our findings of an early TRS in terms of H-donor and H-acceptor hybridizations, this value represents a late TRS for the chemistry around the Zn. We hope to experimentally test this aspect of the model using freeze-quench X-ray absorption spectroscopy, which can measure changes in ligation around the Zn during the reaction with incredible spatial and temporal resolution (34).

1. Cha Y, Murray CJ, Klinman JP (1989) Hydrogen tunneling in enzyme-reactions. *Science* 243:1325–1330.
2. Entwistle ID, Boehm P, Johnstone RAW, Telford RP (1980) Metal-assisted reactions. 8. Selectivity in the reaction of organic halides with tetrahydroborate and the reduction of acyl halides to aldehydes. *J Chem Soc Perk T* 1:27–30.
3. Chancellor T, Quill M, Bergbreiter DE, Newcomb M (1978) Formyl-D aromatic-aldehydes. *J Org Chem* 43:1245–1246.
4. Rafter GW, Colowick SP (1957) Enzymatic preparation of Dpnh and Tpnh. *Method Enzymol* 3:887–890.
5. Klinman JP (1972) Mechanism of enzyme-catalyzed reduced nicotinamide adenine dinucleotide-dependent reductions—Substituent and isotope-effects in yeast alcohol-dehydrogenase reaction. *J Biol Chem* 247:7977–7987.
6. Klinman JP (1976) Isotope-effects and structure-reactivity correlations in yeast alcohol-dehydrogenase reaction—Study of enzyme-catalyzed oxidation of aromatic alcohols. *Biochemistry* 15:2018–2026.
7. Welsh KM, Creighton DJ, Klinman JP (1980) Transition-state structure in the yeast alcohol-dehydrogenase reaction—The magnitude of solvent and alpha-secondary hydrogen isotope effects. *Biochemistry* 19:2005–2016.
8. Rucker J, Cha Y, Jonsson T, Grant KL, Klinman JP (1992) Role of internal thermo dynamics in determining hydrogen tunneling in enzyme-catalyzed hydrogen transfer-reactions. *Biochemistry* 31:11489–11499.
9. Pal S, Park D-H, Plapp BV (2009) Activity of yeast alcohol dehydrogenases on benzyl alcohols and benzaldehydes: Characterization of ADH1 from Saccharomyces carlsbergensis and transition state analysis. *Chem Biol Interact* 178:16–23.
10. Ganzhorn AJ, Green DW, Hershey AD, Gould RM, Plapp BV (1987) Kinetic characterization of yeast alcohol dehydrogenases. Amino acid residue 294 and substrate specificity. *J Biol Chem* 262:3754–3761.
11. Cook PF, Cleland WW (2007) *Enzyme Kinetics and Mechanism* (Taylor & Francis, New York).
12. Frisch MJ, et al. (2004) GAUSSIAN 03 (Gaussian, Inc., Wallingford, CT), revision E.01.
13. Huskey WP, Schowen RL (1983) Reaction-coordinate tunneling in hydride-transfer reactions. *J Am Chem Soc* 105:5704–5706.
14. Huskey WP (1991) Origin of apparent Swain-Schaad deviations in criteria for tunneling. *J Phys Org Chem* 4:361–366.
15. Kohen A, Jensen JH (2002) Boundary conditions for the Swain-Schaad relationship as a criterion for hydrogen tunneling. *J Am Chem Soc* 124:3858–3864.
16. Saunders WH (1985) Calculations of isotope effects in elimination-reactions—New experimental criteria for tunneling in slow proton transfers. *J Am Chem Soc* 107:164–169.
17. Rucker J, Klinman JP (1999) Computational study of tunneling and coupled motion in alcohol dehydrogenase-catalyzed reactions: Implication for measured hydrogen and carbon isotope effects. *J Am Chem Soc* 121:1997–2006.
18. Webb SP, Agarwal PK, Hammes-Schiffer S (2000) Combining electronic structure methods with the calculation of hydrogen vibrational wavefunctions: Application to hydride transfer in liver alcohol dehydrogenase. *J Phys Chem B* 104:8884–8894.
19. Kohen A (2006) *Isotope Effects in Chemistry and Biology*, eds Kohen A, Limbach H-H (Taylor & Francis, Boca Raton), pp. 743–764.
20. Marcus RA (2007) H and other transfers in enzymes and in solution: Theory and computations, a unified view. 2. Applications to experiment and computations. *J Phys Chem B* 111:6643–6654.
21. Nagel ZD, Klinman JP (2006) Tunneling and dynamics in enzymatic hydride transfer. *Chem Rev* 106:3095–3118.
22. Kuznetsov AM, Ulstrup J (1999) Proton and hydrogen atom tunnelling in hydrolytic and redox enzyme catalysis. *Can J Chem* 77:1085–1096.
23. Redington RL (2000) H atom and heavy atom tunneling processes in tropolone. *J Chem Phys* 113:2319–2335.
24. Alhambra C, Corchado JC, Sanchez ML, Gao JL, Truhlar DG (2000) Quantum dynamics of hydride transfer in enzyme catalysis. *J Am Chem Soc* 122:8197–8203.
25. Bigeleisen J (1949) The relative reaction velocities of isotopic molecules. *J Chem Phys* 17:675–678.
26. Anisinov V, Paneth P (2007) ISOEFF 07 (Technical University of Lodz, Lodz, Poland).
27. Cohen-Tannoudji C, Diu B, Laloë F (1977) *Quantum Mechanics* (Wiley, New York).
28. Cook PF, Oppenheimer NJ, Cleland WW (1981) Secondary deuterium and N-15 isotope effects in enzyme-catalyzed reactions—Chemical mechanism of liver alcohol-dehydrogenase. *Biochemistry* 20:1817–1825.
29. Hermes JD, Cleland WW (1984) Evidence from multiple isotope effect determinations for coupled hydrogen motion and tunneling in the reaction catalyzed by glucose-6-phosphate-dehydrogenase. *J Am Chem Soc* 106:7263–7264.
30. Karsten WE, Hwang CC, Cook PF (1999) Alpha-secondary tritium kinetic isotope effects indicate hydrogen tunneling and coupled motion occur in the oxidation of L-malate by NAD-malic enzyme. *Biochemistry* 38:4398–4402.
31. Pudney CR, Hay S, Sutcliffe MJ, Scrutton NS (2006) Alpha-secondary isotope effects as probes of "tunneling-ready" configurations in enzymatic H-tunneling: Insight from environmentally coupled tunneling models. *J Am Chem Soc* 128:14053–14058.
32. Billeter SR, Webb SP, Agarwal PK, Iordanov T, Hammes-Schiffer S (2001) Hydride transfer in liver alcohol dehydrogenase: Quantum dynamics, kinetic isotope effects, and role of enzyme motion. *J Am Chem Soc* 123:11262–11272.
33. Cui Q, Elstner M, Karplus M (2002) A theoretical analysis of the proton and hydride transfer in liver alcohol dehydrogenase (LADH). *J Phys Chem B* 106:2721–2740.
34. Kleifeld O, Frenkel A, Martin JML, Sagi I (2003) Active site electronic structure and dynamics during metalloenzyme catalysis. *Nat Struct Biol* 10:98–103.

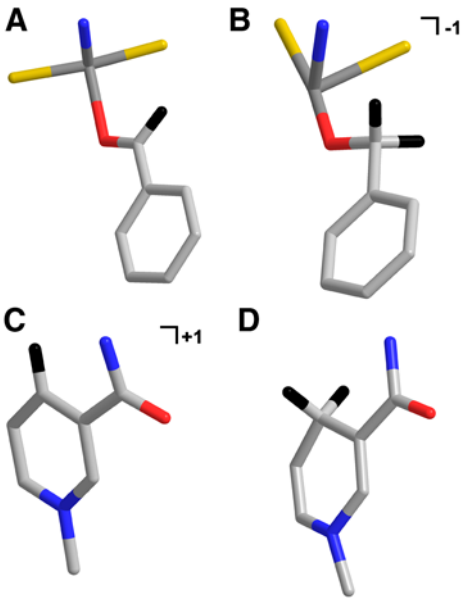

Fig. S1. Optimized reactant and product ground states of the substrate and cofactor showing all heavy atoms and hydrogens of particular interest. (*A*) Benzaldehyde. (*B*) Benzyl alkoxide. (*C*) NAD^+. (*D*) NADH.

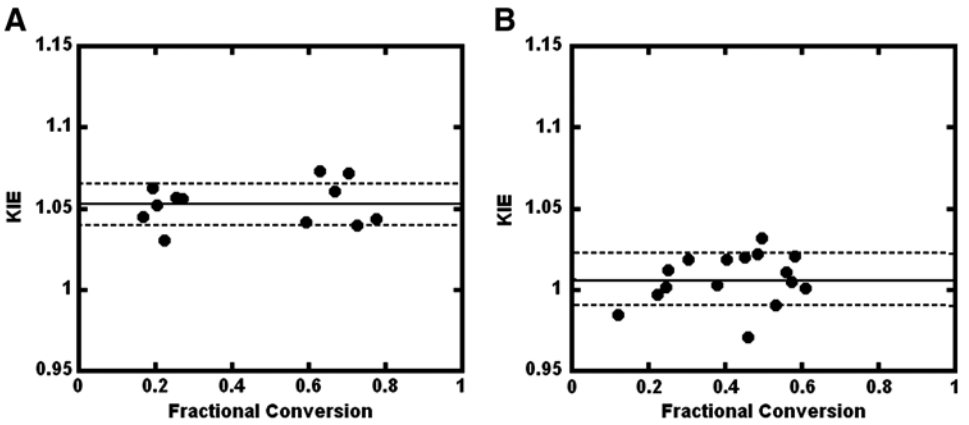

Fig. S2. Measured 2° KIEs for the reduction of benzaldehyde as a function of fractional conversion to products. (*A*) H/*T* with H transfer. (*B*) D/*T* with D transfer. Each data point indicates a single time point during one of two independent reactions (per labeling scheme). The solid line indicates the average value, and the dashed lines are (1σ) above and below the average.